Available online at www.sciencedirect.com
SCIENCE DIRECT
Journal of Magnetic Resonance 181 (2006) 181–190
JMR Journal of Magnetic Resonance
www.elsevier.com/locate/jmr

^{1}H NMR Detection of superparamagnetic nanoparticles at 1 T using a microcoil and novel tuning circuit

Laurel O. Sillerud [a,*], Andrew F. McDowell [b], Natalie L. Adolphi [b], Rita E. Serda [a], David P. Adams [c], Michael J. Vasile [c], Todd M. Alam [d]

[a] *Department of Biochemistry and Molecular Biology, University of New Mexico School of Medicine, Cancer Research and Treatment Center, Albuquerque, NM 87131, USA*
[b] *New Mexico Resonance, 2301 Yale Boulevard SE, Suite C-1, Albuquerque, NM 87106, USA*
[c] *Department of Thin Film, Vacuum and Packaging, MS 1245, Sandia National Laboratories, Albuquerque, NM 87185, USA*
[d] *Department of Electronic and Nanostructured Materials, MS 0886, Sandia National Laboratories, Albuquerque, NM 87185, USA*

Received 12 January 2006; revised 5 April 2006
Available online 15 May 2006

Abstract

Magnetic beads containing superparamagnetic iron oxide nanoparticles (SPIONs) have been shown to measurably change the nuclear magnetic resonance (NMR) relaxation properties of nearby protons in aqueous solution at distances up to ~50 μm. Therefore, the NMR sensitivity for the in vitro detection of single cells or biomolecules labeled with magnetic beads will be maximized with microcoils of this dimension. We have constructed a prototype 550 μm diameter solenoidal microcoil using focused gallium ion milling of a gold/chromium layer. The NMR coil was brought to resonance by means of a novel auxiliary tuning circuit, and used to detect water with a spectral resolution of 2.5 Hz in a 1.04 T (44.2 MHz) permanent magnet. The single-scan SNR for water was 137, for a 200 μs $\pi/2$ pulse produced with an RF power of 0.25 mW. The nutation performance of the microcoil was sufficiently good so that the effects of magnetic beads on the relaxation characteristics of the surrounding water could be accurately measured. A solution of magnetic beads (Dynabeads MyOne Streptavidin) in deionized water at a concentration of 1000 beads per nL lowered the T_1 from 1.0 to 0.64 s and the T_2^* from 110 to 0.91 ms. Lower concentrations (100 and 10 beads/nL) also resulted in measurable reductions in T_2^*, suggesting that low-field, microcoil NMR detection using permanent magnets can serve as a high-sensitivity, miniaturizable detection mechanism for very low concentrations of magnetic beads in biological fluids.

Keywords: NMR; Microcoil; SPION; Permanent magnet; Focused ion beam

1. Introduction

Nuclear magnetic resonance (NMR) spectroscopy is widely used for the real-time identification of chemical compounds in solids, liquids, and gases because it can easily detect and characterize all components of mixtures without requiring separations. Unfortunately, standard high-resolution NMR spectroscopy is not useful for directly detecting dilute biological objects, such as tumor cells, bacteria, bacterial toxins, or viruses, in fluid samples. The weak signals from the analytes in the dilute species are lost against the much stronger background water signal. Even if the dynamic range challenge is met by suppressing the bulk water signal or concentrating the dilute species, the rapid transverse relaxation characteristics of macromolecular, viral, or cellular samples renders their direct detection by NMR difficult. Recent developments involving superparamagnetic iron oxide nanoparticles (SPIONs) have, however, supplied the basis for new applications of NMR with high sensitivity and specificity for the detection and quantitation of dilute biological materials in fluids, such as cancer cells in blood or urine samples, or bacterial contaminants in food products or drinking water.

* Corresponding author. Fax: +1 505 272 6587.
E-mail address: laurel@unm.edu (L.O. Sillerud).

1090-7807/$ - see front matter © 2006 Elsevier Inc. All rights reserved.
doi:10.1016/j.jmr.2006.04.005

SPIONs are enjoying significant uses as biological contrast agents for NMR imaging in human clinical medicine [1,2]. Furthermore, these nanoparticles can be coupled with biologically specific recognition ligands to target epitopes involved in diseases, like cancer. The her-2 protein, for example, is over-produced in many breast cancers and has been the subject of successful NMR imaging experiments where cells displaying this protein have been specifically imaged by means of SPIONs labeled with anti-her-2 antibodies [3]. The image contrast effects due to SPIONs, which are typically embedded in larger beads, rely on the enhancement of the relaxation rates of water molecules surrounding the beads. The magnetic field gradient from a single, micron-sized magnetic bead has been shown to influence the relaxation time T_2^* of the surrounding water within a voxel ~100 μm on a side [4] (a volume of 1 nL), which is ~1000 times larger than that of a single cell. Thus, for a small biological object bound to a magnetic bead in water, the change in the NMR signal caused by the presence of the object is greatly amplified by the effect of the magnetic bead on the surrounding water. Here, we will use the effect of the magnetic beads on the relaxation time T_2^* not for image contrast, but simply as a means of detecting their presence in a small in vitro sample. In principle, a single biological object bound to a magnetic bead can be detected in vitro using a microcoil with a diameter in the 100 μm range, for which the NMR sample volume is similar to that of the volume influenced by a single bead.

In recent years significant advances in the development and fabrication of microcoils (size < 1 mm) for NMR have continued [5–7]. Both planar surface microcoils and solenoidal microcoils have been developed [8–18]. To enhance sensitivity for tiny samples, much of the work with microcoils has utilized the high fields produced by strong superconducting magnets. However, the small size of a microcoil suggests a different possibility: the miniaturization of the magnet, and indeed the entire experiment, through the use of small permanent magnets. While the weaker field of a permanent magnet poses a sensitivity challenge, distortions of the magnetic field due to the proximity of the coil to the sample [19] will be reduced at lower fields. Furthermore, iron oxide particles typically achieve their saturation magnetization in a field of only 0.5–1 T. Thus, for our proposed detection scheme, low-field operation is ideal because it lengthens the T_2^* of the background fluid without reducing the T_2^*-relaxivity of the magnetic beads. Combining microcoil technology with a compact permanent magnet has the added benefits of reducing the cost, maintenance, and space requirements of the NMR system, and enabling portability [20–22]. Our long-range goal is the development of such a portable NMR system capable of detecting minute (even single-particle) quantities of biological materials in fluid samples.

Other workers are currently investigating a number of types of biosensors capable of detecting magnetically labeled cells or molecules [23], including superconducting quantum interference devices (SQUIDs) [24,25], inductive detectors [26], magnetic force microscopy sensors [27] and giant-magnetoresistive (GMR) sensors [28–30]. Recently Grossman et al. [24] achieved a detection limit of $\sim 10^4$ magnetically labeled bacteria using a SQUID system—extrapolating from their results, they predict a detection sensitivity of ~100 bacteria in 1 nL of fluid using a miniaturized SQUID detector. Currently, GMR and magnetic force microscopy based sensors appear to have higher sensitivity, with reports of single particle sensitivity using prototype devices [27,30]. We are motivated to develop a miniaturized NMR system due to the flexibility of this technique. An NMR-based biosensor will also be capable of performing routine relaxation time measurements and low-field spectroscopy, and could be developed further to include diffusion measurements and imaging capabilities with the addition of a miniaturized gradient set [31].

Although low-field, low-frequency, operation of very small microcoils presents special challenges, we report on our initial success with a moderate-size (550 μm diameter) solenoidal microcoil, fabricated by focused gallium-ion beam machining to yield a highly symmetric sample environment. We overcame the challenges of low-frequency microcoil operation by developing a novel tuning circuit. Using this prototype device and magnetic bead solutions containing 1000, 100, and 10 beads per nL, we show that low-field, microcoil NMR T_2^* relaxometry of water can function as a high sensitivity, miniaturizable platform for detecting magnetic beads in fluids. Finally, we outline improvements to the microcoil design that we anticipate will ultimately lead to microcoil NMR detection of a single magnetically labeled biological object in a fluid sample.

2. Materials and methods

2.1. Microcoil fabrication

Microcoils were fabricated [32] onto 2.5-cm long quartz tubes (Vitrocom, Mountain Lakes, NJ) having a 550 μm outer diameter and 400 μm inner diameter using the procedure depicted in Fig. 1. Each tube was cleaned using hydrogen peroxide followed by acetone and isopropyl alcohol. After wet chemical treatment, the tubes were masked on each end, and the 6.2 mm unmasked center targeted for metal deposition was etched for 15 min using a 100 W O_2/Ar plasma. The central region length was chosen based on the coil design with two 2-mm long cuffs on either end. The masked tubes were mounted into individual pin vice fixtures for metal deposition. A stage having eight individual rotation stations contained within a high-vacuum thin film deposition chamber allowed for simultaneous coating of multiple tubes at a constant working distance of 35 cm. Electron beam evaporation was used to deposit a thin Cr layer (200 Å) followed by a relatively thick Au layer (5 μm) around the circumference of the tubes. Deposition rates were chosen to minimize the stress in the layers. After removal of the tubes from the deposition system, the masks were removed using acetone, and the tubes were re-mounted

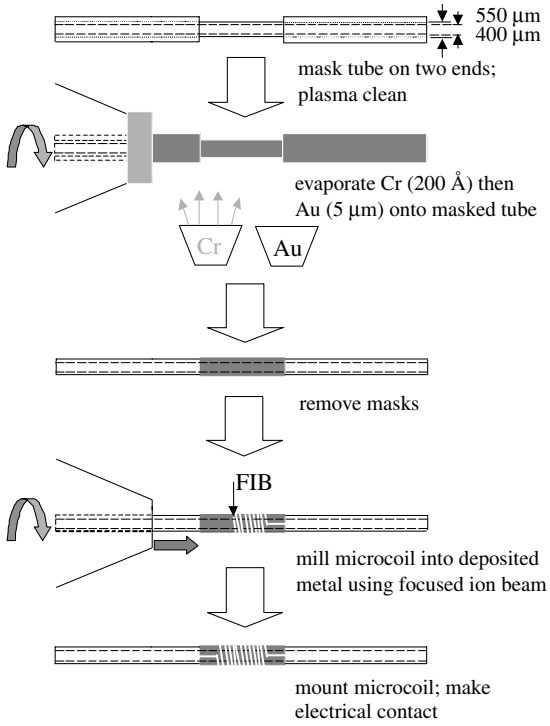

Fig. 1. The sequence of steps used in the fabrication of the microcoil (see text for details).

into pin vice fixtures for rotation within the focused ion beam (FIB) system.

Thirty keV Ga ions emitted from a liquid metal ion source were used to remove the Au/Cr layer in order to define the coil and the neighboring cuffs. The ion beam was focused to approximately 0.5 μm width using a dual-lens Magnum ion column (FEI Co., Hillsboro, OR) and steered across areas outlined by the operator until all the metal was removed from targeted regions. Rates of metal removal were on the order of 10 $\mu m^3/s$ when using a 20 nA Ga beam. Minimal heat and force accompany FIB bombardment. The secondary electron intensity was monitored during ion bombardment to ensure complete removal of metal and slight penetration into the quartz.

An example coil is shown in Fig. 2A with areas removed by the FIB appearing relatively dark due to a low secondary electron intensity. As indicated in Fig. 1 step 4 and the schematic in Fig. 2B, the sample was rotated by an in-vacuum, single-axis rotary stage and translated by a high precision x–y stage along the tube axis in order to define a helix [32]. The motion-control system, consisting of an ultra-high vacuum compatible stepper motor (controlled by a Princeton Research Instruments stepper motor unit) and a reduction gear assembly, could orient a sample with 0.25° precision. This FIB method could likely be extended to fabricate coils onto much smaller tubes having ~50 μm OD.

The finished metal coil used in this work (Fig. 2C) had 28 turns over a length of 2.1 mm. The coil conductors were 65 μm wide with a gap between turns of 10 μm. The sample detection volume within the NMR microcoil was 264 nL. The filling factor was $(400/550)^2 = 53\%$. On the 2-mm long metal cuffs, the FIB removed a 10-μm wide line parallel to the tube axis in order to interrupt conduction. The secondary electron detector within the FIB system also enabled registration of the coil turns. The direct current resistance (Fluke model 179) of the coil was found to be 5.42 Ω. The resistivity of our evaporated Au is 2.898 μΩ-cm (measured on a flat substrate), somewhat higher than bulk Au. Using this value and the geometry of the coil, we calculate a DC resistance of 4.3 Ω. This differs from the measured resistance, perhaps due to contact resistance in the silver epoxy used to attach the coil to the circuit board The microcoil inductance was calculated to be 93 nH.

The coil was packaged using DuPont™ Green Tape™ Low Temperature Co-Fired Ceramic (LTCC) material (DuPont Microcircuit Materials, Research Triangle Park, NC) upon which alloyed gold (Pt/Au) co-firable material (DuPont 5739) solder leads had been plated (Fig. 2D). The coil was secured to the leads, above an opening in the substrate, by means of silver epoxy. This opening assured that the microcoil did not contact the supporting platform and prevented distortion or damage to the very thin metal layer. Mounting the microcoil on a substrate also allowed us to safely manipulate the coil and to attach a fluid transfer line.

2.2. NMR

^{1}H NMR measurements, at a resonant frequency of 44.2 MHz, were performed using a MRTechnology (Tsukuba City, 300-2642 Japan) console, interfaced to a 1.04 T NEOMAX permanent magnet. A smaller 1 T magnet suitable for use in a portable microcoil NMR device could be fabricated. The transmitter pulses were output directly from the console, without a conventional radiofrequency power amplifier, because only 0.25 mW of power was required to produce a B_1 field of 0.3 G (vide infra). Ethanol (100%) was purchased from AAPER (Shelbyville, KY). Spin–lattice ^{1}H T_1 values were obtained, using a standard inversion–recovery sequence, from a Gd-DTPA-doped water sample, from a sample of magnetic beads in water, and from a sample of de-ionized water.

Magnetic beads (Dynabeads MyOne Streptavidin) were purchased from Dynal Inc. Each magnetic bead consists of thousands of 8-nm diameter superparamagnetic iron oxide particles, uniformly dispersed in a polystyrene matrix, and coated with a thin layer of polymer and a monolayer of streptavidin. The beads are 26% Fe by weight (~10% Fe by volume) with an average diameter of 1.05 ± 0.10 μm. The stock solution has a stated bead concentration of between 7×10^3 and 1.2×10^4 beads per nL (equivalent to ~2.6 mg Fe/ml). NMR samples were prepared by diluting the same batch of stock solution with de-ionized water by factors of 10, 100, and 1000 to produce nominal concentrations of 1000, 100, and 10 beads per nL. T_2^* was determined by collecting a single free-induction decay (FID) and fitting the resulting spectrum with a Lorentzian, unless

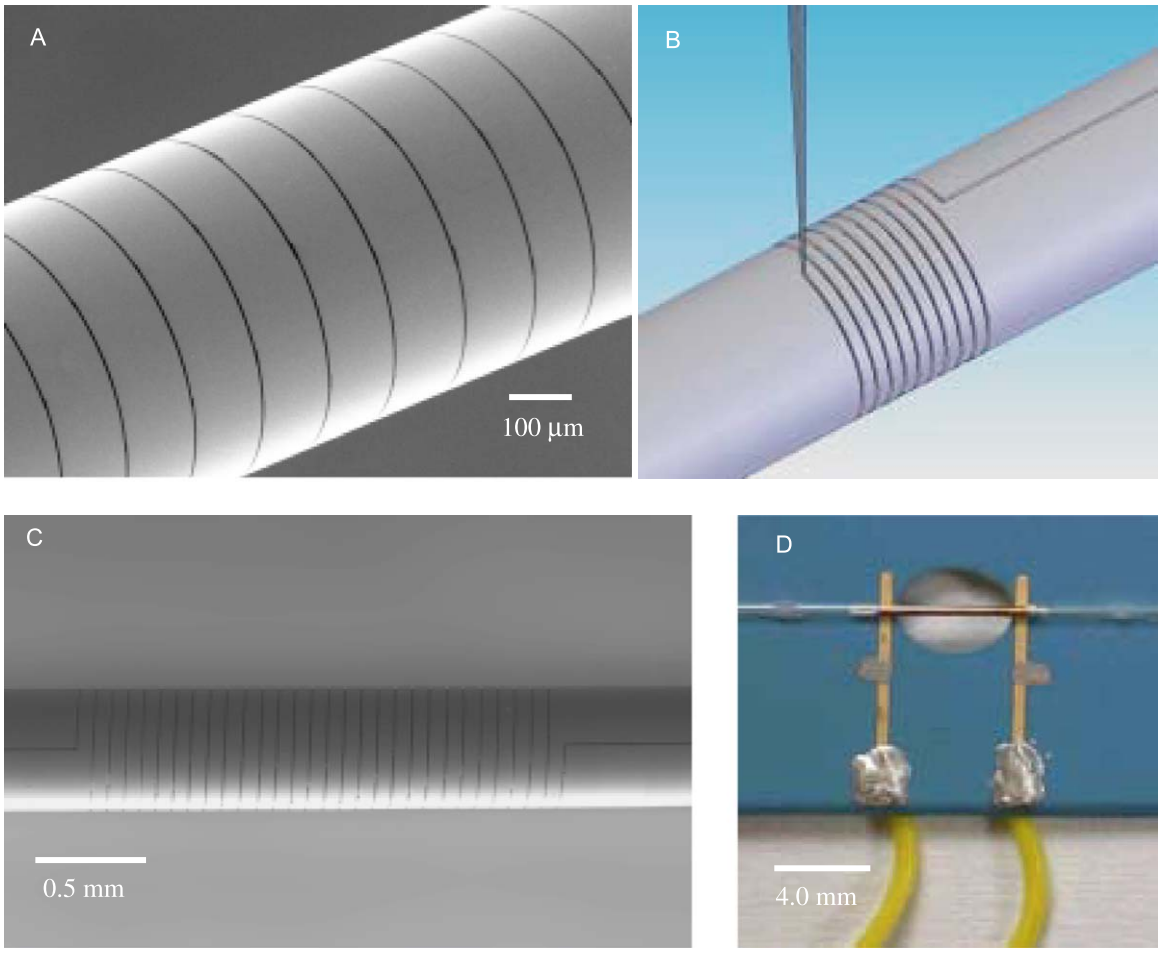

Fig. 2. Focused ion beam lathe machining of the NMR microcoil. (A) Scanning electron micrograph of a coil during the machining process. (B) Schematic of the Ga ion beam machining process. (C) SEM of the coil tested in this work. (D) The finished NMR μ-coil mounted on a low temperature co-fired ceramic substrate with electrical connections.

noted otherwise. The relative shift of the NMR frequency of water caused by the magnetic beads was determined by measuring the resonance frequency of each solution in a 5 mm NMR tube in a conventional coil relative to a separate tube of deionized water. To avoid errors due to field drift of the permanent magnet, each frequency shift measurement was performed by switching several times between the bead solution and a deionized water sample during a period when the frequency drift was confirmed to be <1 Hz/min.

3. Results

3.1. Microcoil tuning

Although the 93 nH inductance of the microcoil could reach resonance at 44.2 MHz with a variable capacitor of reasonable size, we plan to work with much smaller coils in the future. Such small coils are typically operated at higher frequencies [5], where directly resonating the small inductance is feasible. This will not be an option for smaller coils at 44.2 MHz or less, a fact that motivated us to seek alternative ways of tuning the microcoil.

Our tuning solution was to build an auxiliary tank circuit with conventional scale capacitors and to connect the microcoil to it. The key parameter of our microcoil that guided the design of this tuning circuit was its very high resistance. Optimization of a tuned circuit's SNR is a compromise between maximizing coil efficiency, in terms of the magnetic field produced per unit current in the sample coil, while minimizing the resistive noise [33]. The dominant noise source for our very thin, ribbon-wire coils was the large coil resistance [34]. Therefore, the introduction of the additional inductor did not degrade performance, because this extra inductance did not contribute to the resistive losses.

We therefore constructed two circuits for our experiment (Fig. 3). In both cases, the microcoil was mounted by itself in a cast aluminum box, while the external tuning inductor and tuning and matching capacitors were mounted in a separate aluminum box. In the first circuit (Fig. 3A), we used a quarter-wave cable to transform the coil resistance to a higher value and then placed this transformed impedance in parallel with the tuning inductor. In this case, the full resonant voltage was applied to the (transformed) sample coil impedance. In the second circuit (Fig. 3B),

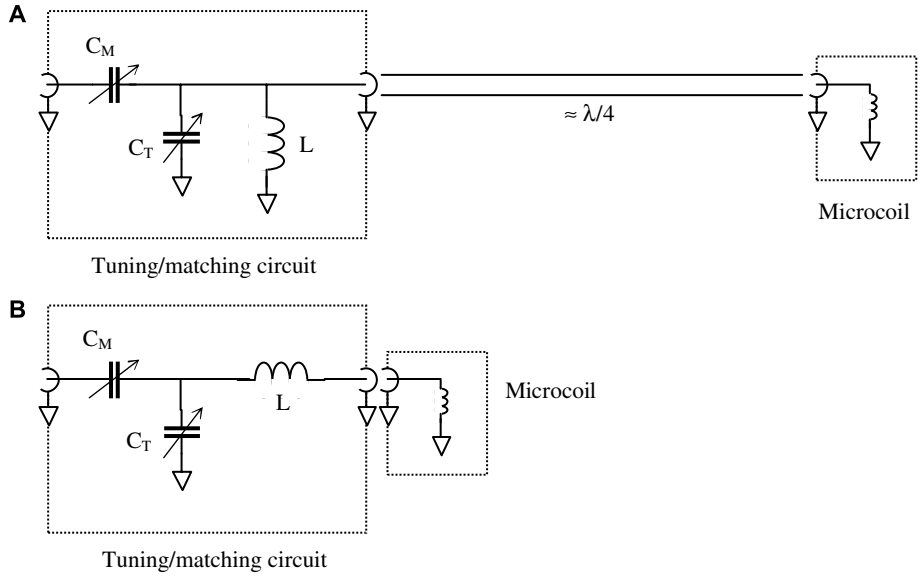

Fig. 3. Probe circuits for tuning low-inductance sample coils at low frequency. In both cases, the microcoil is mounted in its own aluminum box, while the capacitors and large inductor for tuning and matching are mounted in a separate box. The capacitors are adjusted to yield an input impedance of 50 Ω for the combined circuit. In circuit (A), a quarter-wave cable (50 Ω characteristic impedance) transforms the resistance of the microcoil to a larger value, which is placed in parallel with the tuning inductor. In circuit (B), the connection between the two parts of the circuit is short, and the resistance of the microcoil is in series with the tuning inductor. The microcoil is shown as a small inductor; its main function is as a resistor.

the sample coil and tuning inductor were in series, so that all of the resonant current flowed through the sample coil.

The two circuits exhibited nearly identical SNR performance. All subsequent measurements were performed with the first circuit (Fig. 3A), because the remote placement of the tuning and matching elements made it more convenient to work with. The external "tuning" inductor in this circuit was 5 turns of 14 gauge bare copper wire, with a calculated inductance of 0.25 μH, and a calculated resistance at 44.2 MHz of 0.07 Ω. Hence, the tuning inductor contributes negligibly to resistive noise; the tuning circuit is therefore as efficient as a conventional circuit made without the extra tuning inductor. The tuning and matching capacitances were both ~22 pF. The large value of the matching capacitance resulted from the high losses in the microcoil. Because our Wavetek radio frequency sweeper operates at the milliwatt level, and we were reluctant to subject our coil to this power, we estimated the Q of the resonant circuit by constructing a mockup of the microcoil using robust 36 gauge copper wire and a 5 Ω resistor. The mockup circuit had a Q of about 10, as measured from the half-power points on the sweeper output. We also calculated the Q of the coil based on its DC resistance, calculated inductance, and resonance frequency ($Q = \omega L/R$) which gave a similar Q value of 5.

3.2. NMR performance

The nutation performance of the microcoil probe is shown in Fig. 4, where the signal intensity, after an excitation pulse, from a sample of de-ionized water, is plotted as a function of pulse width α. The data followed a typical $\sin(\alpha)$ curve, indicating uniform sample excitation by a homogeneous RF field. The π-pulse width, determined from fitting the sine curve, was 397 ± 4 μs. The transmitter amplitude was 0.32 V (peak-to-peak), corresponding to a power into 50 Ω of only 0.25 mW. A π/2-pulse time of 200 μs corresponds to an RF field strength of 0.3 G, which is produced in our coil by a current of 1.8 mA.

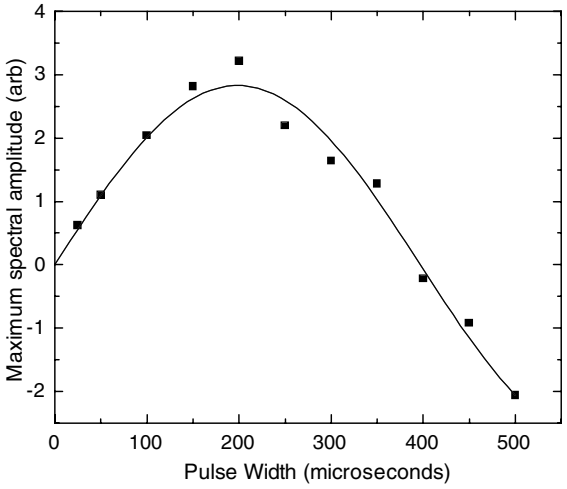

Fig. 4. Determination of the π-pulse width in the μ-coil from a water sample. The spectral intensity is plotted as a function of excitation pulse width. Transmitter power was 0.25 mW. The line is a sine wave fit to the data; the π-pulse length given by this fit is 397 ± 4 μs.

The free-induction decay (FID) and spectrum of deionized water in the microcoil are shown in Fig. 5. The spectrum has a full-width at half maximum (FWHM) of 2.5 Hz. (0.056 ppm) and is reasonably well-fit by a Lorentzian, as shown in the left inset. (At 55% and 11% of maximum, the widths are 2.3 Hz and 8.7 Hz, respectively.)

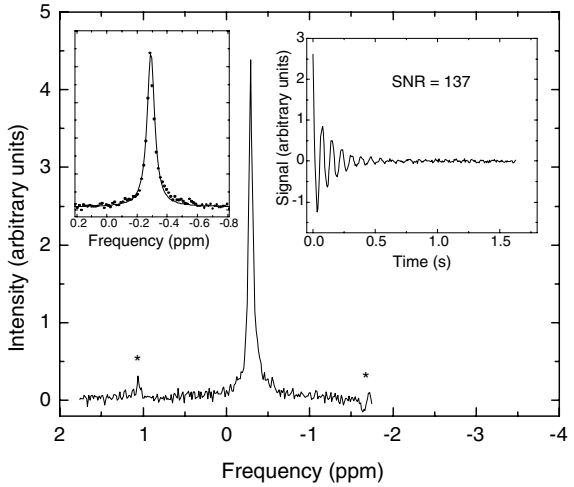

Fig. 5. Absorption spectrum of a sample of de-ionized water, calculated by Fourier-transforming the FID from a single π/2 pulse of width 200 μs. The full width at half maximum is 2.5 Hz, and the line is nearly Lorentzian, as shown by the left inset. The right inset shows the FID. The time domain data were acquired at 200 μs per point and then digitally filtered to 6.4 ms per point (decimated by 32). The signal to noise ratio, measured as the initial FID amplitude divided by the standard deviation of the baseline noise, is 137. The small peaks near −1.7 and +1.1 ppm (marked by ∗) are 60 Hz sidebands of the main peak; they result from gain variations in our receiver.

The SNR after a single π/2 pulse was found to be 137 (ratio of FID amplitude to rms baseline noise). The small sidebands at ±60 Hz were presumably due to gain modulations in our receiver amplifiers, caused by 60 Hz ripple. (Sidebands ±120 Hz were also observed.) Fig. 6 shows the NMR spectrum of a sample of 100% ethanol, calculated from 64 FIDs acquired with a 5 s repetition time. Peaks are seen at $\delta = 1.2$, 3.7, and 5.5 ppm, corresponding to the CH_3—, —CH_2—, and —OH protons, respectively, with

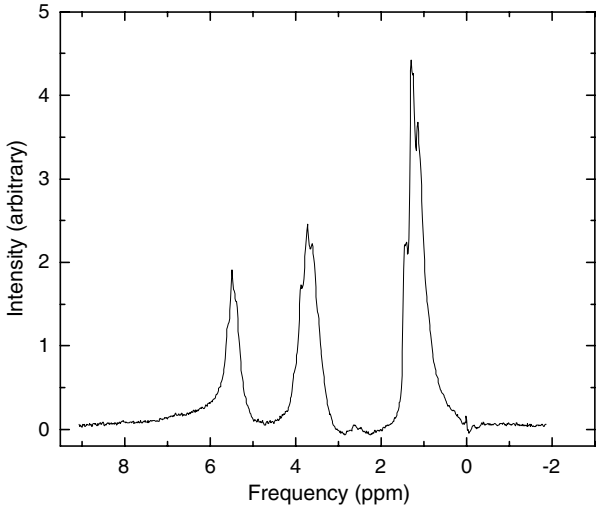

Fig. 6. A spectrum of 100% ethanol taken with 64 FIDs, 8192 pts, 100 μs per point, 10 kHz filters (the lowest available), decimated by 4, with a 5 s relaxation delay. The parameters for a fit of the spectrum to the sum of three Gaussians are listed in Table 1.

Table 1
Fit of the ethanol spectrum to the sum of three Gaussians

δ (ppm)	Multiplicity	Amplitude
1.2 [1.2][a]	[3]	3.0 [3]
3.70 [3.65]	[4]	1.9 [2]
5.48 [5.275]	[1]	1.1 [1]

[a] The standard values are shown in square brackets.

the correct relative amplitudes of 3:2:1 (Table 1). Note also that we can observe the ∼7 Hz J-coupling for the methyl group, and the smaller couplings for the methylene and hydroxyl protons, indicating that the frequency drift over the 5-min experiment was <3 Hz. For both the water and the ethanol experiments, only the X, Y, and Z gradients were shimmed because higher order shims were not available.

To test the ability of the microcoil to measure spin–lattice relaxation times, we used three different water samples; the first was doped with Gd-DTPA to shorten the T_1 to around 70 ms, the second consisted of pure de-ionized water, and the third contained magnetic beads (at a concentration of 1000 beads/nL) in de-ionized water. In all cases, a single scan was acquired at each recovery time. Our results (Fig. 7) show that we can accurately measure relaxation times for both shorter (65 ms) and longer (0.6 and 1.0 s) T_1 values with a standard inversion–recovery pulse sequence. The 397 μs π-pulse gave clean inversion of the magnetization for all samples.

In Fig. 8 we compare the signal detected from deionized water and three different dilutions of the stock Dynabead solution, corresponding to 1000, 100, and 10 beads/nL. The magnitude of each FID is shown, so that they all appear as if they were on resonance. The data are acquired after a single π/2 pulse, digitizing at 100 μs per point (200 μs per point for the deionized water). The data were digitally filtered to achieve an effective digitization time of 400 μs per point. For the 1000 beads/nL sample, 16 FIDs were averaged together; the other data are each a single FID. The beads have two effects on the water spectral peak: the peak broadens and shifts to lower frequencies as the concentration of beads increases. The reduction in T_2^* is apparent in the FIDs. The inset compares the spectra of the four solutions and shows both the linebroadening and the shift to lower frequency caused by the beads. Data for a 1 bead/nL sample (not shown) were indistinguishable from the deionized water data.

The shift of the water resonance to lower frequency in the presence of the paramagnetic beads is not surprising when one considers the lineshape of water in a spherical shell of radius r surrounding a magnetized bead. The lineshape is a uniaxial powder pattern (like that of the chemical shift anisotropy [35]) due to the $3\cos^2\theta - 1$ dependence of the z-component of the dipolar field. The most prominent feature of this lineshape is a cusp at lower frequency, corresponding to spins at $\theta \sim 90$, where the z-component of the bead's magnetic field is negative.

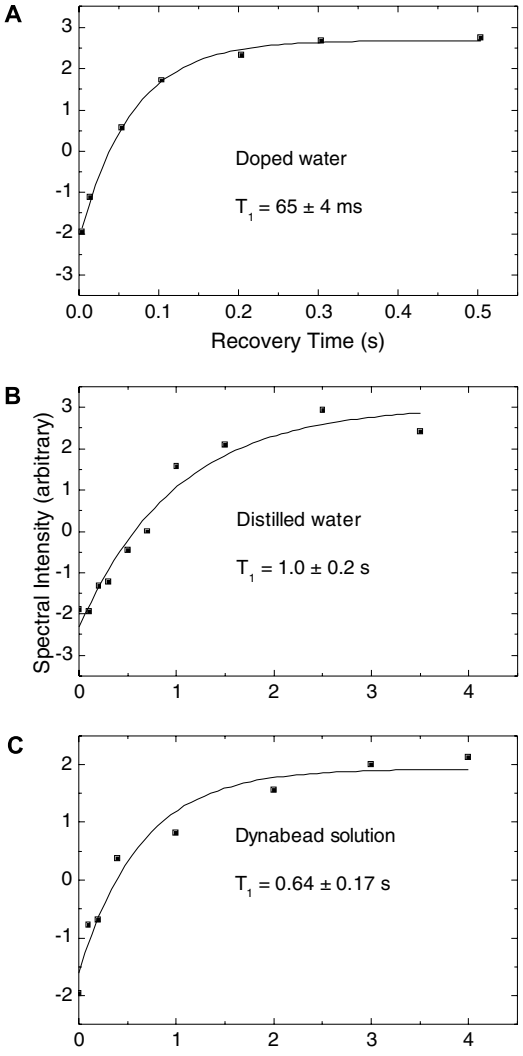

Fig. 7. Measurement of the longitudinal relaxation times for three samples of water in the microcoil. (A) Data from water doped with Gd-DTPA; the T_1 determined was 65 ± 4 ms. (B) Data from de-ionized water; the T_1 determined was 1.0 ± 0.2 s. (C) Data from a 1:10 dilution of Dynabeads in de-ionized water; the T_1 determined was 0.64 ± 0.17 s.

Integrating this lineshape over all r (from $r_{\min}$, at the surface of the bead, to $r_{\max}$, the average distance between beads) results in an approximately Lorentzian lineshape [36].

The solid symbols in Fig. 9A give the observed change in $1/T_2^*(\Delta R_2^*)$ due to the presence of the beads, as a function of bead concentration, C. Here, $\Delta R_2^* = R_2^*{}_{\text{bead solution}} - R_2^*{}_{\text{water}}$, and $R_2^* = \pi\Delta f$, where Δf is the FWHM in Hz of the Lorentzian line [37] fit to each spectrum in Fig. 8. Note that both axes in Fig. 9A are logarithmic; the straight line (drawn as a guide to the eye) has a slope of roughly 2/3 indicating that $\Delta R_2^* \propto C^{2/3}$ over this range of concentrations. The relaxivity $r_2^*(= \Delta R_2^*/C)$ is therefore not a constant, but decreases with increasing concentration as shown in Fig. 9B.

Because magnetic field gradients can cause motion of the magnetic beads with respect to the fluid, it was not clear a priori that the concentration of beads delivered to the microcoil would be the same as the concentration in the supply syringe. Indeed, the measured T_2^* of bead solutions

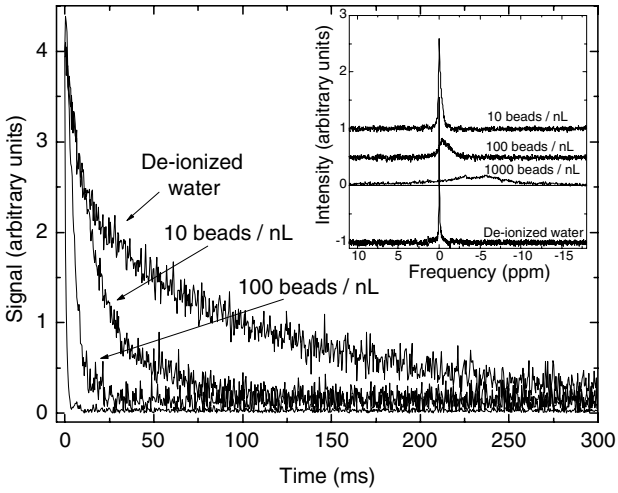

Fig. 8. Effect of SPIONs (Dynabeads) on the transverse (T_2^*) relaxation time of water in the microcoil. The first 300 ms of the free induction decays for the de-ionized water sample, as well as water samples containing 10, 100, and 1000 beads/nL (not labeled), are shown. For the first three samples, a single scan, digitally filtered to an effective acquisition rate of 400 μs per point, is shown. For the 1000 beads/nL sample, 16 scans were averaged together. The inset shows the ^{1}H NMR spectra from the FIDs, showing both the increase in line width and the shift to lower frequency due to the presence of the magnetic beads.

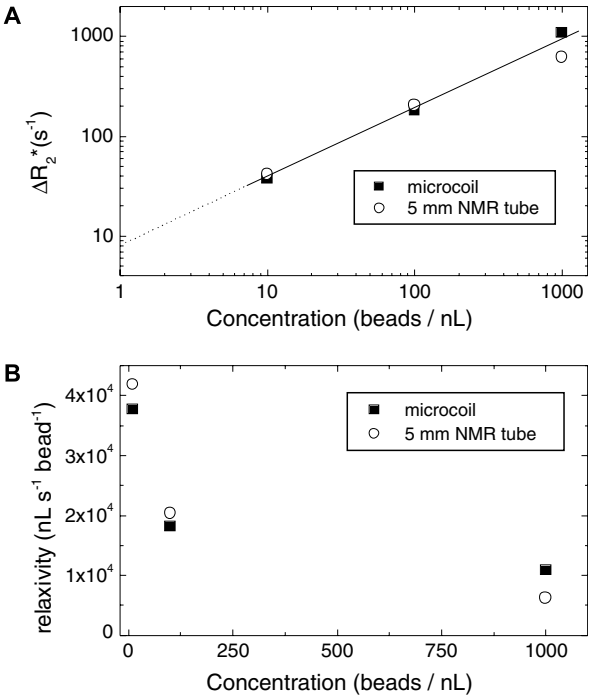

Fig. 9. (A) Change in $1/T_2^*$ due to the presence of 1 μm magnetic beads as a function of concentration. The solid squares are data obtained using a 264 nL microcoil, while the open circles are data obtained from the same bead solutions in 5 mm NMR tubes using a conventional probe. The straight line, drawn as a guide to the eye, has a slope of roughly 2/3 on this log-log plot, indicating that ΔR_2^* is proportional to the 2/3 power of concentration over this range. (B) Relaxivity r_2^* of the magnetic beads as a function of concentration. Per bead, the enhancement of $1/T_2^*$ increases with decreasing concentration.

in the microcoil was observed to decrease over time if the bead solution was allowed to sit motionless in the coil over several minutes, suggesting that the spatial distribution of the beads was changing, due to clustering, settling, or migration out of the coil. Thus, in order to validate the microcoil results, we measured the T_2^* of the same bead solutions (1000, 100, and 10 beads/nL) and deionized water in capped 5 mm NMR tubes using a conventional probe in the same magnet. Each measurement was performed within 20–30 s after shaking the tube to homogenize the bead solution, and the tube was immediately extracted afterwards to visually confirm that the beads had not settled during the measurement. (Shimming was performed on the deionized water, and a sample holder was used to position the other 5 mm tubes identically, to avoid the need to re-shim. Repeatedly placing the same sample in the probe using this holder gave linewidths that were reproducible to ±5 Hz.) Migration of the beads was similarly observed in the 5 mm tubes (both visually and as an increase in T_2^* over time) if the samples were allowed to sit in the magnet for longer time periods. The ΔR_2^* values measured for the bead solutions in 5 mm tubes (open symbols in Fig. 9A) are in good agreement with those obtained for the same concentrations in the microcoil, indicating that the expected concentrations were delivered to the microcoil.

4. Discussion

The rapid expansion of biomedical applications for magnetic nanoparticles motivates a concomitant development of the means for detecting small numbers of these intriguing agents. The most challenging goal is the detection of a single cell or molecule labeled with one magnetic bead. As discussed above, MR imaging studies [4] indicate that one bead can measurably influence the water signal in a region of length scale 100 μm surrounding the bead. Hence an NMR microcoil of diameter and length of this size (i.e., a sample volume of ~1 nL) should be optimal for detecting a single magnetic bead in an in vitro sample. A coil of this size opens up the possibility of a readily portable NMR system based on a small permanent magnet, as long as the challenges of operating a microcoil at low frequencies can be met.

We have demonstrated that a novel tuning circuit, capable of tuning an arbitrarily small inductance at a frequency compatible with a permanent magnet, coupled with a medium sized microcoil, allows spectroscopic and relaxation measurements using less than 1 mW of radiofrequency power. (This low power requirement further aids in making the NMR system portable.) The line widths for deionized water are adequate for the detection of magnetic beads in water at a concentration of 10 beads/nL. The coil used for these proof-of-principle measurements is not well optimized for NMR sensitivity, as discussed further below. However, our first results indicate that this approach will allow the detection of very dilute biological species, perhaps as rare as a single cell or molecule labeled with a single magnetic bead.

The challenge of achieving this detection sensitivity can be discussed quantitatively in light of the data of Figs. 8 and 9. We envision that in a portable system, a fluid containing very dilute, magnetically labeled biological objects flows through a ~1 nL coil while the FID is monitored. The challenge is to detect the difference between the FID of the background fluid and the same fluid containing one magnetic bead within the coil volume. Considering Fig. 8, we see that we can readily detect the change in T_2^* of water due to 10 beads/nL, or roughly 3000 magnetic beads in our current prototype microcoil (264 nL volume). If we can achieve a similar T_2^* for deionized water (~100 ms) and adequate SNR in a coil with a 1 nL sample volume, we should easily be able to detect 10 beads.

Extrapolating the straight line in Fig. 9A suggests that the ΔR_2^* of one bead in a 1 nL volume is ~8 s^{-1}, which would have caused an increase in the linewidth of water in our current microcoil from ~3 to ~6 Hz. This increase should have been detectable given our high SNR. The fact that we did not detect a change in line width due to the 1 bead/nL solution suggests that the ΔR_2^* for this concentration is lower than that predicted by extrapolating the straight line in Fig. 9A. A theoretical treatment of dipolar broadening of the NMR line due to dilute magnetic impurities [36] indicates that the linewidth will be proportional to $C^{1/2}$ at higher concentrations and will be linear in C at lower concentrations. Our slope of 2/3 suggests that we are in the transition region between these two limits, and we should expect a higher slope at lower concentration, resulting in a predicted value of ΔR_2^* lower than 8 s^{-1} at 1 bead/nL. Hence, the detection of a single 1-μm Dynabead in a 1 nL coil will require that we achieve an even narrower line width, while at the same time detecting adequate signal strength.

A 100 μm diameter coil (1 nL) will give substantially less signal than our 264 nL coil due to the reduced sample size. Thus we must consider whether such a coil will have sufficient SNR to detect 10 beads in its 1 nL volume. In the "large" microcoil data in Fig. 8, we can maximize our detection sensitivity by integrating the FIDs, say from 50 to 300 ms, which is roughly equivalent to applying strong digital filtering. These integral values are 397 and 122 (arbitrary units), for the water and 10 beads/nL data, respectively. The uncertainty in these values is 3, which corresponds to a signal to noise ratio (SNR) of 133 for determining the amplitude of the water signal. The smaller 1 nL volume coil will have much less signal, but also less noise (due to its lower resistance). For microcoils in the limit where skin depth is small compared to wire size (which is not quite true for our coil), the SNR per unit volume scales as the inverse of the coil diameter.[34] Hence, the absolute SNR scales as the square of the linear dimension of the sample. We are proposing to scale the sample and coil dimension down by roughly a factor of 6, so we expect that the SNR in the determination of the integrated water signal amplitude will be about 3.7. Hence, the 1 nL coil will require that the beads change the area under the

FID of the background water by at least 25%. Here, a concentration of 10 bead/nL caused a 70% change in the integrated signal from 50 to 300 ms, and is therefore expected to remain detectable in the 1 nL coil, assuming we achieve a similar background water T_2^*.

While our current prototype coil is already capable of detecting the presence of as few as 3000 magnetic beads, it has not been optimized for maximal SNR performance for operation at 44.2 MHz. The thickness of the coil "wire" is much less than a skin depth, which raises the resistance of the coil without providing any improvements in signal detection. The width of the "wire" is much more than a skin depth, so that it may be possible to increase the number of turns per unit length and gain in coil sensitivity without suffering a nullifying increase in resistance. Careful attention to the geometrical design of our next, smaller coil, should improve the SNR above the estimate of ~3.7 based on this first attempt. SNR performance will be enhanced by reducing the coil resistance, which is higher than expected in our first ion-milled coil. Improving the line width of the background fluid places a lower demand on the SNR performance. The use of susceptibility matching (either in the choice of evaporated metals or via a matching fluid) and the reduction of the filling factor (by increasing the relative wall thickness in the capillary tube) are known to improve the line widths in small coils [19]. In addition, the magnet we have used is not very homogeneous and only first order shims are available; a more homogeneous applied field may be required to achieve narrower lines. Future work in optimizing the coil will also include comparisons of both the SNR and line width performance of ion-milled coils to other types of microcoils, such as copper wire-wound coils. We anticipate that some compromise between line width and sensitivity will provide the best opportunity for detecting single biological objects.

The surface of a single cancer cell (~10 μm in diameter) can bear upwards of 10^5 binding sites (antigens) for a particular antibody [38] and can accommodate up to 400 1-μm diameter magnetic beads, assuming monolayer coverage and random close packing. Thus we believe that sensitivity to 10 beads would already be adequate to detect single magnetically labeled cells. On the other hand, bacterial toxin molecules (e.g., botulism toxin) are much smaller and would accommodate only one or a few beads, requiring single-bead detection sensitivity. Hence, single-bead sensitivity remains our ultimate goal.

So far, our discussion of detection limits has been based on measurements of a particular type (Dynabeads) and size (1 μm) of magnetic bead. Larger magnetic beads (having larger magnetic moments) are available and will allow us to increase the relaxivity of a single bead and further lower our detection limit. Shapiro et al. [4] observed a T_2^* of ~14 ms from single 1.63 μm diameter Bangs microbeads in 1 nL image voxels. Assuming that their background T_2^* was at least 100 ms, we calculate ΔR_2^* for a single 1.63 μm bead in a 1 nL volume to be at least 60 s^{-1}, which should be readily detected using a 1 nL microcoil with a background water T_2^* of 100 ms and a SNR of ~3. Even larger beads (e.g., 2.8-μm and 4.8-μm Dynabeads) are commercially available, and may be used, if necessary, to further enhance our ability to detect a single magnetic bead in an NMR microcoil.

Acknowledgments

The authors gratefully acknowledge the efforts of K. Peterson and G.M. Schwartz for packaging and V. Carter Hodges for technical assistance. We would also like to thank Dr. M.S. Conradi for helpful suggestions and Dr. Eiichi Fukushima for his careful reading of the manuscript. Sandia National Laboratories is a multiprogram laboratory operated by Sandia Corporation, a Lockheed Martin Company, for the United States Department of Energy's National Nuclear Security Administration under Contract DE-AC04-94AL-85000. This research was supported in part by LDRD funds from Sandia National Laboratories. R.E.S. was supported by an NIH pre-doctoral fellowship.

References

[1] C.A. Taschner, S.G. Wetzel, M. Tolnay, J. Froehlich, A. Merlo, E.W. Radue, Characteristics of ultrasmall superparamagnetic iron oxides in patients with brain tumors, Am. J. Roentgenol. 185 (2005) 1477–1486.
[2] M.G. Harisinghani, M. Saksena, R.W. Ross, S. Tabatabaei, D. Dahl, S. McDougal, R. Weissleder, A pilot study of lymphotrophic nanoparticle-enhanced magnetic resonance imaging technique in early stage testicular cancer: a new method for noninvasive lymph node evaluation, Urology 66 (2005) 1066–1071.
[3] D. Artemov, N. Mori, B. Okollie, Z.M. Bhujwalla, MR molecular imaging of the Her-2/neu receptor in breast cancer cells using targeted iron oxide nanoparticles, Magn. Reson. Med. 49 (2003) 403–408.
[4] E.M. Shapiro, S. Skrtic, K. Sharer, J.M. Hill, C.E. Dunbar, A.P. Koretsky, MRI detection of single particles for cellular imaging, Proc. Natl. Acad. Sci. USA 101 (2004) 10901–10906.
[5] M.E. Lacey, R. Subramanian, D.L. Olson, A.G. Webb, J.V. Sweedler, High-resolution NMR spectroscopy of sample volumes from 1 nl to 10 ml, Chem. Rev. 99 (1999) 3133–3152.
[6] K.R. Minard, R.A. Wind, Solenoidal microcoil design, Part I: optimizing rf homogeneity, Concepts Magn. Reson. 13 (2001) 128–142.
[7] K.R. Minard, R.A. Wind, Solenoidal microcoil design, Part II: Optimizing winding parameters for maximum signal-to-noise performance, Concepts in Magn. Reson. 13 (2001) 190–210.
[8] J.D. Trumbull, I.K. Glasgow, D.J. Beebe, R.L. Magin, Integrating microfabricated fluidic systems and NMR spectrscopy, IEEE Transactions on Biomedical Engineering 47 (2000) 3–7.
[9] A.M. Wolters, D.A. Jayawickrama, C.K. Larvie, J.V. Sweedler, Capillary isotachophoresis/NMR: extension to trace impurity analysis and improved instrument coupling, Anal. Chem. 74 (2002) 2306–2313.
[10] A.M. Wolters, D.A. Jayawickrama, J.V. Sweedler, Microscale NMR, Curr. Opin. Chem. Biol. 6 (2002) 711–716.
[11] B. Sorli, J.F. Chateaux, M. Pitival, H. Chahboune, B. Favre, A. Briguet, P. Morin, Micro-spectrometer for NMR: analysis of small quantities in vitro, Meas. Sci. Technol. 15 (2004) 877–880.
[12] J.H. Walton, J.S. de Roop, M.V. Shutov, A.G. Goloshevky, M.J. McCarthy, R.L. Smith, S.D. Collins, A micromachined double-tuned NMR microprobe, Anal. Chem. 75 (2003) 5030–5036.
[13] J. Dechow, A. Forchel, T. Lanz, A. Haase, Fabrication of NMR-microsensors for nanoliter sample volumes, Micoelectron. Eng. 53 (2000) 517–519.

[14] S. Eroglu, B. Gimi, B. Roman, G. Friedman, R.L. Magin, NMR spiral surface microcoils: design, fabrication and imaging, Concepts Magn. Reson. B 17 (2003) 1–10.
[15] C. Massin, G. Boero, F. Vincent, J. Abenhaim, P.-A. Besse, R.S. Popovic, High-q factor rf planar microcoils for micro-scale NMR spectroscopy, Sensors Actuators A 97–98 (2002) 280–288.
[16] C. Massin, F. Vincent, A. Homsy, K. Ehrmann, G. Boero, P.-A. Besse, A. Daridon, E. Verpoorte, N.F. de Rooij, R.S. Popovic, Planar microcoil-based microfluidic NMR probes, J. Magn. Reson. 164 (2003) 242–255.
[17] J.A. Rogers, R.J. Jackman, G.M. Whitesides, D.L. Olson, J.V. Sweedler, Using microcontact printing to fabricate microcoils on capillaries for high resolution proton nuclear magnetic resonance on nanoliter volumes, Appl. Phys. Lett. 70 (1997) 2464–2466.
[18] V. Malba, R. Maxwell, L.B. Evans, A.F. Bernhardt, M. Cosman, K. Yan, Laser-lathe lithography—a novel method for manufacturing nuclear magnetic resonance microcoils, Biomed. Microdevices 5 (2003) 21–27.
[19] A.G. Webb, S.C. Grant, Signal-to-noise and magnetic susceptibility trade-offs in solenoidal microcoils for NMR, J. Magn. Reson. B 113 (1996) 83–87.
[20] G. Moresi, R.L. Magin, Miniature permanent magnet for table-top NMR, Concepts Magn. Reson. B 19 (2003) 35–43.
[21] H. Wensink, D.C. Hermes, A. van den Berg, High signal to noise ratio in low-field NMR on a chip: simulations and experimental results, in: 17th IEEE MEMS, 2004, pp. 407–410.
[22] A.G. Goloshevsky, J.H. Walton, M.V. Shutov, J.S. de Ropp, S.D. Collins, M.J. McCarthy, Development of low field nuclear magnetic resonance microcoils, Rev. Sci. Inst. 76 (2005) 024101.
[23] N. Pamme, Magnetism and microfluidics, Lab Chip 6 (2006) 24–38.
[24] Y.R. Chemla, H.L. Grossman, Y. Poon, R. McDermott, R. Stevens, M.D. Alper, J. Clarke, Ultrasensitive magnetic biosensor for homogeneous immunoassay, Proc. Natl. Acad. Sci. USA 97 (2000) 14268–14272.
[25] H.L. Grossman, W.R. Myers, V.J. Vreeland, R. Bruehl, M.D. Alper, C.R. Bertozzi, J. Clarke, Detection of bacteria in suspension by using a superconducting quantum interference device, Proc. Natl. Acad. Sci. USA 101 (2004) 129–134.
[26] M. Lany, G. Boero, R.S. Popovic, Superparamagnetic microbead inductive detector, Rev. Sci. Instr. 76 (2005) 084301.
[27] Y. Amemiya, T. Tanaka, B. Yoza, T. Matsunaga, Novel detection system for biomolecules using nano-sized bacterial magnetic particles and magnetic force microscopy, J. Biotechnol. 120 (2005) 308–314.
[28] D.L. Graham, H.A. Ferreira, P.P. Freitas, Magnetoresistive-based biosensors and biochips, Trends Biotechnol. 22 (2004) 455–462.
[29] J. Shotter, P.B. Kamp, A. Becker, A. Puhler, G. Reiss, H. Bruckl, Comparison of a prototype magnetoresistive biosensor to standard fluorescent DNA detection, Biosens. Bioelectron. 15 (2004) 1149–1156.
[30] D.L. Graham, H.A. Ferreira, P.P. Freitas, J.M. Cabral, High sensitivity detection of molecular recognition using magnetically labeled biomolecules and magnetoresistive sensors, Biosens. Bioelectron. 18 (2003) 483–488.
[31] D.A. Seeber, J.H. Hoftiezer, W.B. Daniel, M.A. Rutgers, C.H. Pennington, Triaxial magnetic field gradient system for microcoil magnetic resonance imaging, Rev. Sci. Instr. 71 (2000) 4263–4272.
[32] M.J. Vasile, C. Biddick, S. Schwalm, Microfabrication by ion milling: the lathe technique, J. Vac. Sci. Technol. B 12 (1994) 2388.
[33] D.I. Hoult, R.E. Richards, The signal-to-noise ratio of the nuclear magnetic resonance experiment, J. Magn. Reson. 24 (1976) 71–85.
[34] T.L. Peck, R.L. Magin, P.C. Lauterbur, Design and analysis of microcoils for NMR microscopy, J. Magn. Reson. B 108 (1995) 114–124.
[35] C.P. Slichter, Principles of Magnetic Resonance, third ed., Springer-Verlag, New York, 1989, p. 609.
[36] A. Abragam, Principles of Nuclear Magnetism, Clarendon Press, Oxford, 1961, pp. 125–128.
[37] E. Fukushima, S.B.W. Roeder, Experimental Pulse NMR: A Nuts and Bolts Approach, Addison-Wesley, Reading, MA, 1981, p. 138.
[38] P.M. Smith-Jones, S. Vallabahajosula, S.J. Goldsmith, V. Navarro, C.J. Hunter, D. Bastidas, N.H. Bander, In vitro characterization of radiolabeled monoclonal antibodies specific for the extracellular domain of prostate-specific membrane antigen, Cancer Res. 60 (2000) 5237–5243.